Optica Applicata, Vol. LII, No. 4, 2022
DOI: 10.37190/oa220409

Demonstration of a high extinction ratio TiN-based TM-pass waveguide polarizer

Zhuan Zhao[1,2,*], Giovanni Santi[3], Alain Jody Corso[4], Maria Guglielmina Pelizzo[1]

[1]Department of Information Engineering, University of Padova, Via Gradenigo 6/B, 35131, Padova, Italy

[2]School of Physics and Materials Science, Guangzhou University, Guangzhou 510006, China

[3]Centro di Ateneo di Studi e Attività Spaziali (CISAS), Università di Padova, via Venezia, 15, 35131, Padova, Italy

[4]Istituto di Fotonica e Nanotecnologie (CNR-IFN), Consiglio Nazionale delle Ricerche, via Trasea, 7, 35131 Padova, Italy

[*]Corresponding author: zhuan.zhao@studenti.unipd.it

A high extinction ratio transverse magnetic (TM)-pass plasmonic waveguide polarizer has been designed and optimized. This device exploits two parallel TiN strips embedded in a silicon dioxide cladding to cut off the transverse electric (TE) polarization state, which is either reflected or absorbed, while the TM mode can pass through the main silicon waveguide with significant low losses. Given a device of 5 μm length, an extinction ratio as high as 60.7 dB and an insertion loss of 2.23 dB were achieved at the target wavelength of 1.55 μm. To our knowledge, this extinction ratio is one of the highest values ever reported. In the wavelength of 1.45–1.59 μm, the proposed device provides an optical bandwidth of 140 nm for an extinction ratio more than 30 dB and an insertion loss less than 3 dB. This device is relatively simple and is easier to be fabricated than other architectures that are found in the literature.

Keywords: plasmonic waveguide polarizer, extinction ratio, insertion loss, broadband.

1. Introduction

Photonic integrated circuits (PICs) based on silicon attracts widespread interest for their suitability in many applications, such as optical sensing and communication [1,2], quantum photonics [3], and nonlinear optics [4]. This is mainly due to their compatibility with conventional CMOS technologies, high processing control, low cost, and high volume manufacturing. Most of these photonic devices are based on the silicon on insulator (SOI) technology, which exploits light confinement in a Si waveguide de-

posited onto SiO_2 structure, and that is embedded in a cladding material, typically SiO_2 or air [5]. The high index-contrast between the silicon core and the cladding material enables the high-density integration of photonic components and generally introduces significant polarization dependence [6]. This feature causes the polarization-sensitive issues such as polarization mode dispersion (PMD), polarization dependent loss (PDL), and polarization dependent wavelength shift (PDWS) [7], degrading their practical performance, especially in the devices and systems operating with a single polarization (SP) such as on-chip photonic building blocks [8], fiber-optic gyroscope, and electro-optic switching arrays [9]. Any deterioration in the purity of the operating polarization may result in significant performance degradation. Therefore, precise control of the polarization state of light is necessary in these optical circuits integration. As a simple and efficient solution, polarizers are among the most important components for realizing high-dense PICs since their anisotropic behavior, which results in suppressing the undesired polarization state and making the desired one pass through.

When dealing with polarizers, the key features which must be taken into consideration are low insertion loss (IL), high extinction ratio (ER), compact footprint and ease of manufacture. So far, various types of polarizers based on different concepts have been proposed. An example of TE-pass polarizer based on shallowly-etched SOI ridge waveguide has been proposed by DAI *et al*. [10], where an extinction ratio as high as 25 dB over a 100 nm wavelength range has been achieved with a 1 mm-long polarizer. Also, TE and TM polarizers can be realized through sub-wavelength grating waveguides (SWG), where the SWG is designed to specifically support Bloch mode for one polarization state, which can in turn propagate with low losses, while working as a Bragg reflector for the orthogonal one, that is consequently reflected. For example, GUAN *et al*. [11] fabricated and experimentally verified a TM-pass SWG of 9 μm length with measured extinction ratio of 27 dB and the less loss of 0.5 dB at the central wavelength 1550 nm. Another SWG was reported by XIONG *et al*., which realizes an extinction ratio 30 dB and an average insertion loss of 0.4 dB [12], but with a relative long device length of 60 μm. In recent years, surface plasmon polaritons (SPPs) opened up the possibility to achieve ultracompact devices. Many different designs have been proposed, such as metal–insulator–metal (MIM) structures [7, 13–15], directional couplers (DCs) [16–18] and hybrid plasmonic waveguides (HPWs) [19]. Polarizers based on special materials such as graphene [20–23], and vandium dioxide (VO_2) [24] are also reported. However, the graphene-based polarizer faced some uncertainties in the experiment, such as the shape, size, number of layers, and purity of graphene [25]. VO_2 as a phase-change material (PCM) needs a cooling process to return its insulating phase, whose phase-transition is volatile [26]. On the other hand, titanium nitride (TiN) turns out to have many advantages, such as high thermal stability, bio-compatibility and manufacturability by epitaxial growth on a large number of substrates [27], and it is in turn a CMOS compatible material; it is, indeed, already employed in HPWs. An example of TM-pass plasmonic polarizer has been proposed by AZZAM and OBAYYA [28], which provides an insertion loss of 1 dB and an ER of 20 dB at a 2.84-μm-long device. However, this

extinction ratio is relatively low compared to previously mentioned designs. A lower extinction ratio increases the power penalty (PP), and the 0 and 1 levels get closer during transmission process, which degrades the bit-error ratio (BER), while the insertion loss (IL) does not degrade the BER directly, the BER is typically impacted by the insertion loss deviation (ILD) of all the optical components in a device and system. Thus, a higher extinction ratio is urgently needed to reduce the number of errors and improve transmission efficiency [29,30]. Moreover, this TiN-based TM-pass polarizer uses a thin silicon dioxide layer surrounding the silicon core and uses air as cladding, which is challenging to be manufactured.

In this work, a different design of the TM-pass hybrid plasmonic waveguide polarizer is presented. The main contribution of this work is using two symmetrical TiN strips covered with SiO_2 cladding to form the hybrid plasmonic waveguide. Such structure allows to achieve remarkable performance in an ultra-compact device, and it is relatively easy to be manufactured. By choosing geometrical parameters appropriately, the resulting device realizes an extinction ratio as high as 60.7 dB and an insertion loss of 2.23 dB in a device length of only 5 μm. To the best of our knowledge, an ER of 60.7 dB is an outstanding value. In addition, benefiting from this design, a broad bandwidth of 140 nm is realized for an ER more than 30 dB and an IL less than 3 dB.

2. Design and modelling

The proposed TM-pass hybrid plasmonic waveguide (HPW) polarizer and its cross- sectional view along the coupling are shown in Fig. 1. A silicon waveguide of width w and height h is placed on top of the 2 μm thick SiO_2 substrate, as in a typical SOI platform. Two TiN strips of width w_1, height h_1 and length L are placed sideways parallel to the main waveguide and separated by a distance g. A subsequent SiO_2 cladding was deposited to cover the whole structure. The two TiN strips act as the attenuation of the

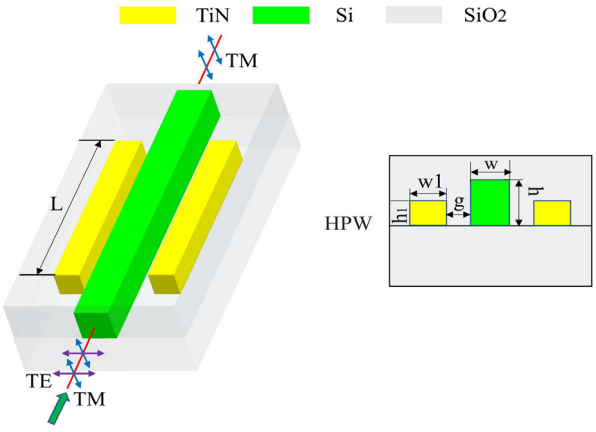

Fig. 1. Concept and cross-section view of the proposed TM-pass waveguide.

TE-mode propagating in the silicon waveguide. Consequently, if the strips are long enough, the TE-mode is fully absorbed. On the other hand, the TM-mode can propagate on the Si waveguide with a small attenuation.

The optimization of this device is carried out using the Wave Optics Module of COMSOL Multiphysics [31] via a finite element method (FEM). Both 2D and 3D simulations are performed at the target wavelength of 1.55 μm, because it provides minimal attenuation (<0.2 dB/km) for fiber-optic communications. The refractive index of Si and SiO_2 considered in this work are 3.478 [32] and 1.444 [33], respectively. While at the working wavelength, SiO_2 and Si have real refraction index, TiN has both a real and imaginary component, retrieved by the following dielectric function [34]:

$$\varepsilon(w) = \varepsilon_b - \frac{\omega_p^2}{\omega(\omega + i\gamma_p)} + \frac{f_1\omega_1^2}{\omega_1^2 - \omega^2 - i\omega\gamma_1} \tag{1}$$

where $\varepsilon_b = 2.485$, $\omega_p = 5.953$ eV, $\omega_1 = 3.954$ eV, $\gamma_p = 0.5142$ eV, $\gamma_1 = 2.4852$ eV, and $f_1 = 2.0376$.

Firstly, a 2D simulation has been carried out to determine the optimal dimensions w and h of the central Si waveguide without considering the lateral TiN strips. Afterwards, 3D simulations have been used for the optimization of the TiN strips dimension $h_1 \times w_1 \times L$ and their distance g from Si waveguide. The boundary conditions of 3D model are depicted in Fig. 2, port 1 is selected for exciting waves with TE and TM modes, and port 2 is selected as wave exit, while the remaining 4 surfaces are imposed with a scattering boundary condition. A physics-controlled normal mesh is employed for the whole structure, pursuing the target value of extinction ratio (ER) and insertion loss (IL) defined as:

$$\mathrm{ER} = 10\log_{10}\frac{P_{TM}}{P_{TE}} \tag{2}$$

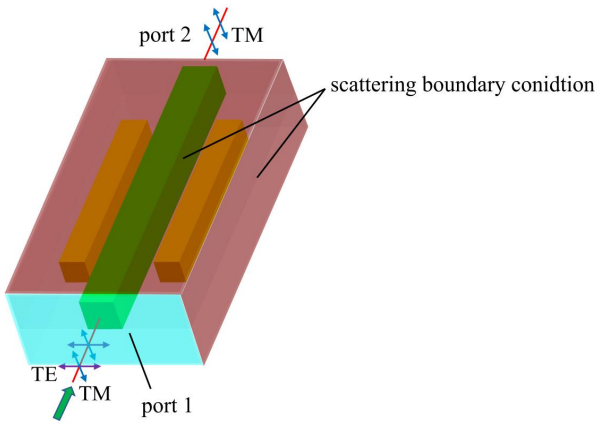

Fig. 2. The boundary conditions for 3D simulations.

$$\mathrm{IL} = -10\log_{10}\frac{P_{\mathrm{TM}}}{P_{\mathrm{input}}} \tag{3}$$

where P_{TM} and P_{TE} are the TM and TE output powers, respectively, and P_{input} is the input one. An efficient TM-pass polarizer requires the TE mode to be attenuated as much as possible while the TM mode propagates with minimal losses. Such requirement results in a high extinction ratio and a simultaneously low insertion loss. Assuming w_1 set to 1 μm, which is a value large enough to induce the plasmonic effect, the 3D simulation goal is to find the optimal gap g between TiN strip and Si core, the length L of TiN strips, and the thickness h_1 of TiN strips. The initial work is the sweep of L, g, and h_1 parameters in a larger step (see Table 1), searching for the promising solution evaluated by the criteria: ER ≥ 30 dB, IL ≤ 3 dB. Then a more detailed scan is performed in the promising areas to find the optimal solution.

T a b l e 1. Sweeping ranges used for the optimization of structure.

Parameters	Sweeping range	Step
L	[1, 5] μm	1 μm
g	[10, 210] nm	20 nm
h_1	[10, 300] nm	5 nm

3. Results and discussion

Figure 3 reports the mode effective refractive index n_{eff} computed for the TE and TM polarization states varying both the Si waveguide width and height from 100 to 400 nm. Such simulations support the selection of the dimension of the Si waveguide in order to allow the propagation of both TE and TM modes. A mode can propagate along the waveguide if its effective refractive index is greater than that of the cladding material, which is 1.44 for this case. In figure, TM mode is always at a cut-off when

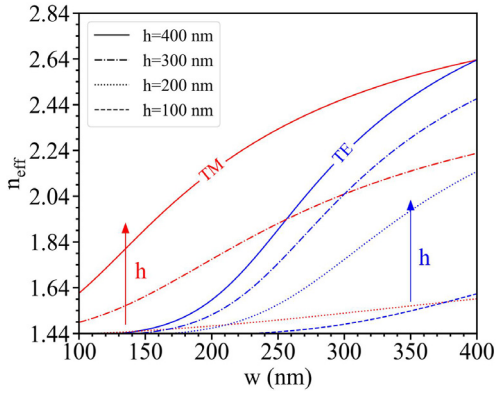

Fig. 3. TE and TM effective refractive index of the Si waveguide *versus* width w computed for four different heights.

h is 100 nm, while a height greater than 300 nm allows its propagation. Regarding the TE mode, it propagates for all *h* values only when the waveguide width is larger than approximately 250 nm.

A value of 220 nm is adopted in the present study, as such number is commonly used in SOI devices because of the numerous projects carried out in wafer foundries [35]. Moreover, AZZAM and OBAYYA [28] report considerable results obtained with a TiN-based TM-pass plasmonic polarizer having the silicon waveguide width of such size. Waveguide height between 300 and 400 nm are also very common value in SOI devices; for instance, some polarization beam splitters [36–38] and TM-pass polarizer [39] have been proven to perform well with a height of 340 nm. At this height, both TM and TE propagates.

Figure 4 reports the ER and the IL *versus* the three geometrical parameters *L*, *g* and h_1 for a fixed width and height value $w = 220$ nm and $h = 340$ nm, respectively. The gap *g* between TiN strips and Si waveguide ranges with a step of 20 nm, while the strip height h_1 ranges with a step of 10 nm. Dots refer to values obtained with sampling step reduced to 5 nm. Different graphs correspond to the TiN strip lengths *L* ranging from 2 to 5 μm. For a given strip length *L*, the IL decreases as the gap *g* increases; this behaviour can be explained considering that the TM-component propagating in the

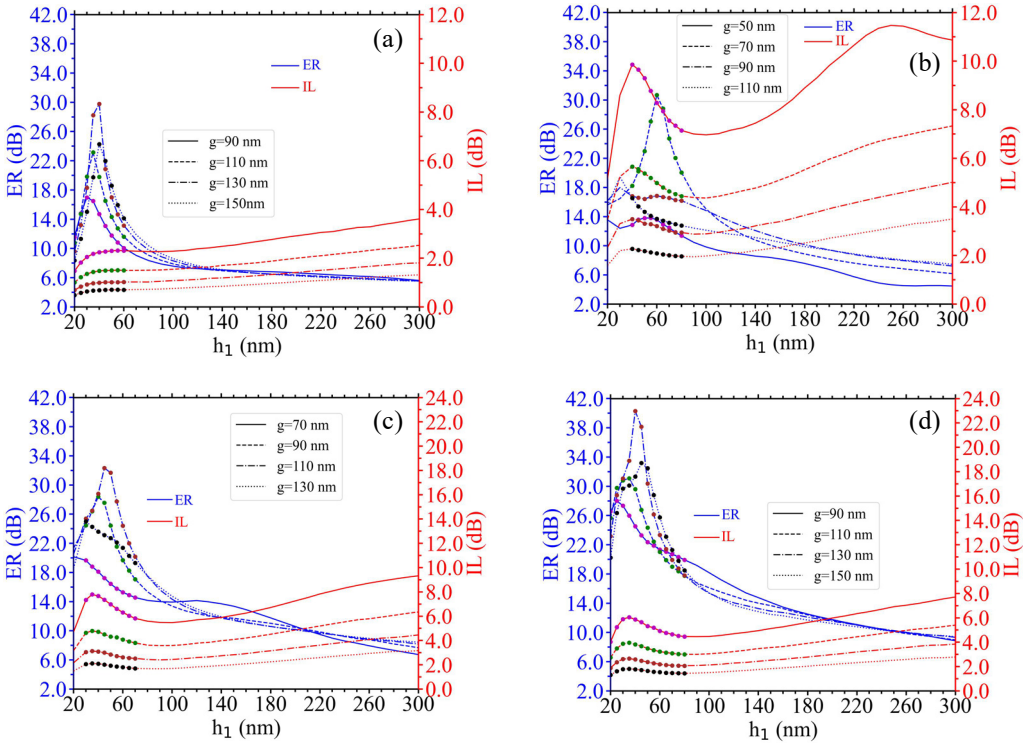

Fig. 4. Extinction ratio and insertion loss *versus* free geometrical parameters: (a) $L = 2$ μm, (b) $L = 3$ μm, (c) $L = 4$ μm, (d) $L = 5$ μm, and $w = 220$ nm, $h = 340$ nm.

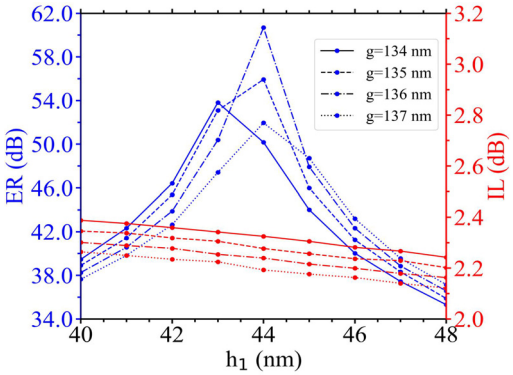

Fig. 5. Extinction ratio and insertion loss *versus* free geometrical parameter in the promising areas: L = 5 μm, w = 220 nm, h = 340 nm.

SiO_2 slightly interacts with the TiN strips and both TiN-Si strips gap g and length L of TiN strips increase the propagation losses for TM. For given L and g values, the IL generally increases as the h_1 increases, although the curve initially shows a local maximum peak.

A different behaviour characterized the ER *versus* h_1 curve, as for a given L it shows a global maximum for any g. The promising solution of initial work is obtained at the peak ER of Fig. 4(d), realizing an ER of 40.3 dB and an IL of 2.58 dB. In Fig. 5 a more detailed analysis around the peak ER at the g of 130 nm is reported by minimizing the variation step of g and h_1 into 1 nm (see Table 2). Finally, the optimal structure has been selected based on the criteria: ER ≥ 30 dB, IL ≤ 3 dB (see Fig. 5), being that realizing an ER of 60.7 dB and an IL of 2.23 dB with L = 5 μm, g = 136 nm, and h_1 = 44 nm.

T a b l e 2. Sweeping ranges used for the optimization of structure.

Promising solution	Sweeping ranges
L = 5 μm, g = 130 nm, h_1 = 40 nm	g: [110, 150] nm, h_1: [30, 50] nm

Figure 6 shows the electrical field distribution of TE and TM mode for both the dielectric waveguide (DW) and hybrid plasmonic waveguide (HPW), as well as the TE and TM mode power transmission flow from top view. The DW is formed by embedding a Si waveguide in a SiO_2 cladding, and the HPW is formed by implanting two TiN strips in the DW. It is vividly shown that the optical filed of TM mode in DW is mainly confined in silicon waveguide while in HPW it experienced a little bit loss since the slight interaction with TiN strips. In contrast, the optical field of TE mode in DW is mainly distributed in SiO_2 cladding, while in HPW it experienced a large mode distribution mismatch since the hybrid plasmonic effect, which further induces significant reflection loss. When TM/TE mode transmission power is launched at the input port, the TE mode is quickly eliminated while TM mode is passed with a small amount of attenuation.

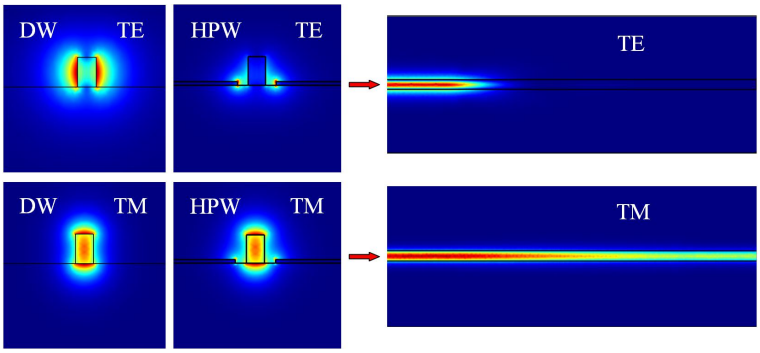

Fig. 6. The electrical field distribution of TE and TM mode for both the DW and HPW, as well as the TE and TM mode power transmission flow from top view, for optimal structure.

A comparison of this nominal performance with the TM-pass waveguide polarizers experimental (E) and theoretical (T) results available in literature is summarized in Table 3. WU *et al*. [40], SABER *et al*. [41], and PRAKASH *et al*. [42] reported a high extinction ratio TM-pass polarizer, respectively, but their designs are very challenging to fabricate. Moreover, WU *et al*. suffered from a relatively long device length (*i.e.* 30 μm). HU *et al*. [43] and YUAN *et al*. [44] reported a TM-pass waveguide polarizer with an ER of 40 and 45 dB, respectively; nevertheless, they are not CMOS compatible.

T a b l e 3. Nominal performance compared with TM-pass polarizer reported in literature.

	E/T	ER [dB]	IL [dB]	Length [μm]	Bandwidth [nm]	CMOS compatiblity
GUAN *et al.* [11]	E	27	0.5	9	60	Yes
SANCHEZ *et al.* [24]	T	15	3	1	60	Yes
AZZAM *et al.* [28]	T	20	1	2.84	Not mentioned	Yes
BAI *et al.* [39]	T	25.6	0.088	2.5	Not mentioned	No
WU *et al.* [40]	T	51.83	0.08	30	61	Yes
SABER *et al.* [41]	T	45.4	1.7	8.8	72	Yes
PRAKASH *et al.* [42]	T	45	0.6	5	120	Yes
HU *et al.* [43]	T	40	3	150	200	No
YUAN *et al.* [44]	T	45	1	7.5	120	No
ZHOU *et al.* [45]	E	40	0.4	12.9	24	Yes
XU *et al.* [46]	T	31.63	0.18	5.2	155	Yes
RUI *et al.* [47]	T	28.3	0.4	10	65	No
SABER *et al.* [48]	T	30.11	3.08	15	21.5	Yes
KIM *et al.* [49]	E	34	1	4	200	Yes
ZHANG *et al.* [50]	T	24	0.97	12	110	Yes
ELKADER *et al.* [51]	T	22	0.11	1	260	Yes
DHINGRA *et al.* [52]	T	38	0.05	20	200	Yes
GUAN *et al.* [53]	E	15.2	0.84	3.9	100	No
This work	**T**	**60.7**	**2.23**	**5**	**140**	**Yes**

ZHOU *et al.* [45] fabricated a TM-pass polarized with a extinction ratio of 40 dB, but this design is based on a hyperuniform disordered photonic structure (HUDPS) in which the fabrication process is time-consuming and probably expensive, making it difficult to commercialize. On the contrary, this work realizes an ER as high as 60.7 dB in a compact length of only 5 μm and it is relatively easy to realize. Thus, the proposed structure is candidate to provide the highest ER ever reported in a very compact device.

A further feature which may be of interest is the spectral performance. The ER and IL of the optimal structures are investigated in the wavelength region that ranges from 1.45 to 1.65 μm (Fig. 7). It is found that the optimal structure performs well in a broadband wavelength range. For example, using the criteria: ER ≥ 30 dB and IL ≤ 3 dB, the wavelength guarantees this performance ranges from 1.45 to 1.59 μm, which is over 140 nm.

In evaluating the performance of the promising structures, it is needed to consider the challenges in manufacturing. Therefore, the tolerances of the optimal structure are investigated. It is worth noting that strips length L is relatively easy to guarantee from

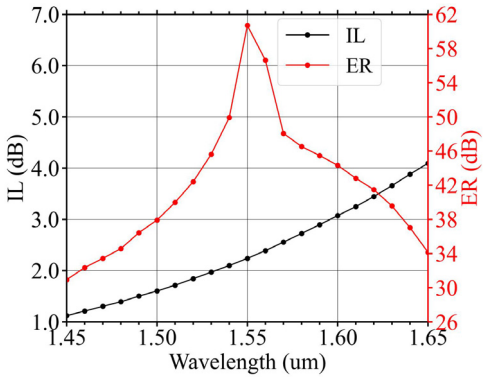

Fig. 7. The IL and ER as a function of wavelength for optimal structure.

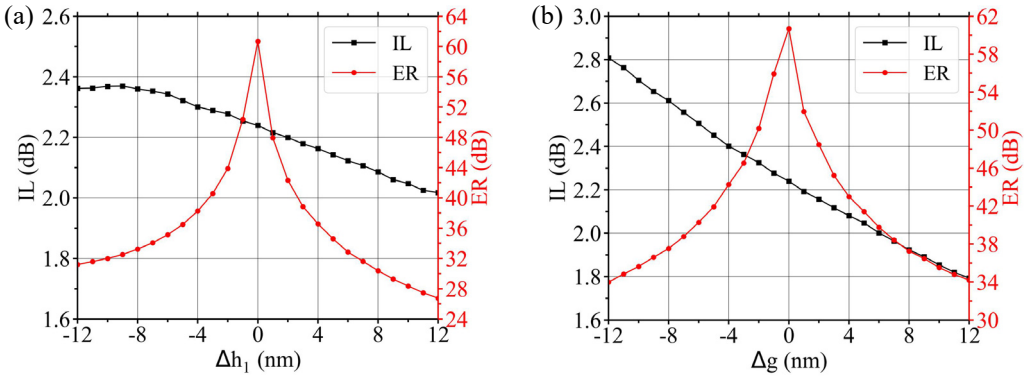

Fig. 8. The sensitivity of extinction ratio and insertion loss to free parameters g and h_1. Panels (a) and (b) present the results for optimal structure.

the manufacturing perspective, so only the variations of g and h_1 are considered. ER and IL values for changes of g and h_1 within 12 nm of each nominal value are reported in Fig. 8. It can be seen that the IL gradually decreases as both the g and h_1 increase, actually being more sensitive to g than h_1. The ER initially increases, peaks at a certain value and then falls. The optimal structure realizes the largest ER of 60.7 dB and an IL of 2.23 dB at the nominal value of g and h_1. Let's still considering the criteria that previously established, variations of g and h_1 to the nominal value that can guarantee such performance are range from –12 to 12 nm and –12 to 8 nm, respectively.

The optimal structure could be fabricated on a SOI wafer and a specific fabrication process can be described as follows: first, a photoresist layer is spin-coated on the SOI substrate, and electron-beam lithography (EBL) [54] or 193 nm DUV lithography [55] is used to define the waveguide pattern, followed by a plasma reactive ion etching (RIE) process to obtain the whole silicon waveguide. Then a TiN layer is deposited by plasma-assisted atomic layer deposition (PAALD) [56] or plasma-enhanced atomic layer deposition (PEALD) [57] while retaining the photoresist. A subsequent layer of photoresist is spray-coated for EBL to define TiN strip patterns. Then, an etching process removes all the photoresists. Finally, the structure is covered with a SiO_2 cladding by plasma-enhanced chemical vapor deposition (PECVD) [54]. Different SOI wafers typically have a different non-uniformity for the silicon layer thickness. For example, 200 mm wafers have a non-uniformity with a 3σ of ±6 nm [58], but 300 mm wafers with a 3σ of ±1 nm is realized [59]. The linewidth uniformity in the 193 DUV lithograph process is controlled with a 3σ of ±8 nm [60]. These variations significantly impact the performance of the device. However, in the proposed device, all the free parameters exhibit a tolerance over 16 nm, which enables high-quality fabrication.

4. Conclusion

In this work, a CMOS compatible TM-pass waveguide polarizer has been proposed and optimized at the target wavelength of 1.55 μm. Both 2D simulation and 3D simulation have been taken into consideration. The nominal performance required for the considered device is a higher extinction ratio and a lower insertion loss.

The optimal structure with the g = 136 nm, h_1 = 44 nm, and L = 5 μm is selected, which realized an extinction ratio as high as 60.7 dB and an insertion loss of 2.23 dB. This extinction ratio is one of the highest values ever reported in a 5 μm device length. The spectral performance and sensitivity of the optimal structure is also investigated. These evaluations are based on the criteria: ER ≥ 30 dB and IL ≤ 3 dB. The wavelength that can provide such performance ranges from 1.45 to 1.59 μm. The robustness performance remains acceptable when the g, h_1 range from –12 to 12 nm and –12 to 8 nm, respectively.

Through analysis, this structure is relatively compact and easy to be fabricated, thus providing a good application prospect for high-dense PLCs.

Reference

[1] Barwicz T., Watts M.R., Popović M.A., Rakich P.T., Socci L., Kärtner F.X., Ippen E.P., Smith H.I., *Polarization-transparent microphotonic devices in the strong confinement limit*, Nature Photonics **1**, 2007, pp. 57–60, DOI: 10.1038/nphoton.2006.41.

[2] Wu L., Guo J., Xu H., Dai X., Xiang Y., *Ultrasensitive biosensors based on long-range surface plasmon polariton and dielectric waveguide modes*, Photonics Research **4**(6), 2016, pp. 262–266, DOI: 10.1364/PRJ.4.000262.

[3] Silverstone J.W., Bonneau D., Ohira K., Suzuki N., Yoshida H., Iizuka N., Ezaki M., Natarajan C.M., Tanner M.G., Hadfield R.H., Zwiller V., Marshall G.D., Rarity J.G., O'Brien J.L., Thompson M.G., *On-chip quantum interference between silicon photon-pair sources*, Nature Photonics **8**, 2014, pp. 104–108, DOI: 10.1038/nphoton.2013.339.

[4] Liu X., Osgood R.M., Vlasov Y.A., Green W.M.J., *Mid-infrared optical parametric amplifier using silicon nanophotonic waveguides*, Nature Photonics **4**, 2010, pp. 557–560, DOI: 10.1038/nphoton.2010.119.

[5] Dai D., Liu L., Gao S., Xu D.X., He S., *Polarization management for silicon photonic integrated circuits*, Laser & Photonics Reviews **7**(3), 2013, pp. 303–328, DOI: 10.1002/lpor.201200023.

[6] Dai D., Liu L., Wosinski L., He S., *Design and fabrication of ultra-small overlapped AWG demultiplexer based on α-Si nanowire waveguides*, Electronics Letters **42**(7), 2006, pp. 400–402, DOI: 10.1049/el:20060157.

[7] Huang Y., Zhu S., Zhang H., Liow T.-Y., Lo G.-Q., *CMOS compatible horizontal nanoplasmonic slot waveguides TE-pass polarizer on silicon-on-insulator platform*, Optics Express **21**(10), 2013, pp. 12790–12796, DOI: 10.1364/OE.21.012790.

[8] Zafar H., Odeh M., Khilo A., Dahlem M.S., *Low-loss broadband silicon TM-pass polarizer based on periodically structured waveguides*, IEEE Photonics Technology Letters **32**(17), 2020, pp. 1029–1032, DOI: 10.1109/LPT.2020.3011056.

[9] Chen C.-H., Pang L., Tsai C.-H., Levy U., Fainman Y., *Compact and integrated TM-pass waveguide polarizer*, Optics Express **13**(14), 2005, pp. 5347–5352, DOI: 10.1364/OPEX.13.005347.

[10] Dai D., Wang Z., Julian N., Bowers J.E., *Compact broadband polarizer based on shallowly-etched silicon-on-insulator ridge optical waveguides*, Optics Express **18**(26), 2010, pp. 27404–27415, DOI: 10.1364/OE.18.027404.

[11] Guan X., Chen P., Chen S., Xu P., Shi Y., Dai D., *Low-loss ultracompact transverse-magnetic-pass polarizer with a silicon subwavelength grating waveguide*, Optics Letters **39**(15), 2014, pp. 4514–4517, DOI: 10.1364/OL.39.004514.

[12] Xiong Y., Xu D.-X., Schmid J.H., Cheben P., Ye W.N., *High extinction ratio and broadband silicon TE-pass polarizer using subwavelength grating index engineering*, IEEE Photonics Journal **7**(5), 2015, article no. 7802107, DOI: 10.1109/JPHOT.2015.2483204.

[13] Ying Z., Wang G., Zhang X., Huang Y., Ho H.-P., Zhang Y., *Ultracompact TE-pass polarizer based on a hybrid plasmonic waveguide*, IEEE Photonics Technology Letters **27**(2), 2015, pp. 201–204, DOI: 10.1109/LPT.2014.2365029.

[14] Ng T.K., Khan M.Z.M., Al-Jabr A., Ooi B.S., *Analysis of CMOS compatible Cu-based TM-pass optical polarizer*, IEEE Photonics Technology Letters **24**(9), 2012, pp. 724–726, DOI: 10.1109/LPT.2012.2187329.

[15] Wang J., Qi M., Xuan Y., Huang H., Li Y., Li M., Chen X., Jia Q., Sheng Z., Wu A., Li W., Wang X., Zou S., Gan F., *Proposal for fabrication-tolerant SOI polarization splitter-rotator based on cascaded MMI couplers and an assisted bi-level taper*, Optics Express **22**(23), 2014, pp. 27869–27879, DOI: 10.1364/OE.22.027869.

[16] Ni B., Xiao J., *Plasmonic-assisted TE-pass polarizer for silicon-based slot waveguides*, IEEE Photonics Technology Letters **30**(5), 2018, pp. 463–466, DOI: 10.1109/LPT.2018.2798709.

[17] NI B., XIAO J., *A compact silicon-based TE-pass polarizer using three-guide directional couplers*, IEEE Photonics Technology Letters **29**(19), 2017, pp. 1631–1634, DOI: 10.1109/LPT.2017.2739242.
[18] GUAN H., NOVACK A., STRESHINSKY M., SHI R., FANG Q., LIM A.E.-J., LO G.-Q., BAEHR-JONES T., HOCHBERG M., *CMOS-compatible highly efficient polarization splitter and rotator based on a double -etched directional coupler*, Optics Express **22**(3), 2014, pp. 2489–2496, DOI: 10.1364/OE.22.002489.
[19] ALAM M.Z., AITCHISON J.S., MOJAHEDI M., *Compact and silicon-on-insulator-compatible hybrid plasmonic TE-pass polarizer*, Optics Letters **37**(1), 2012, pp. 55–57, DOI: 10.1364/OL.37.000055.
[20] KIM J.T., CHOI C.-G., *Graphene-based polymer waveguide polarizer*, Optics Express **20**(4), 2012, pp. 3556–3562, DOI: 10.1364/OE.20.003556.
[21] GUAN C., LI S., SHEN Y., YUAN T., YANG J., YUAN L., *Graphene-coated surface core fiber polarizer*, Journal of Lightwave Technology **33**(2), 2015, pp. 349–353, DOI: 10.1109/JLT.2014.2386893.
[22] YIN X., KE X., CHEN L., ZHANG T., LI J., ZHU Z., LI X., *Ultra-broadband TE-pass polarizer using a cascade of multiple few-layer graphene embedded silicon waveguides*, Journal of Lightwave Technology **34**(13), 2016, pp. 3181–3187, DOI: 10.1109/JLT.2016.2547896.
[23] BAO Q., ZHANG H., WANG B., NI Z., LIM C.H.Y.X., WANG Y., TANG D.Y., LOH K.P., *Broadband graphene polarizer*, Nature Photonics **5**, 2011, pp. 411–415, DOI: 10.1038/nphoton.2011.102.
[24] SÁNCHEZ L., LECHAGO S., SANCHIS P., *Ultra-compact TE and TM pass polarizers based on vanadium dioxide on silicon*, Optics Letters **40**(7), 2015, pp. 1452–1455, DOI: 10.1364/OL.40.001452.
[25] ZHANG S., LI Z., XING F., *Review of polarization optical devices based on graphene materials*, International Journal of Molecular Sciences **21**(5), 2020, article no. 1608, DOI: 10.3390/ijms21051608.
[26] CARRILLO S.G.-C., NASH G.R., HAYAT H., CRYAN M.J., KLEMM M., BHASKARAN H., WRIGHT C.D., *Design of practicable phase-change metadevices for near-infrared absorber and modulator applications*, Optics Express **24**(12), 2016, pp. 13563–13573, DOI: 10.1364/OE.24.013563.
[27] KINSEY N., FERRERA M., NAIK G.V., BABICHEVA V.E., SHALAEV V.M., BOLTASSEVA A., *Experimental demonstration of titanium nitride plasmonic interconnects*, Optics Express **22**(10), 2014, pp. 12238 –12247, DOI: 10.1364/OE.22.012238.
[28] AZZAM S.I., OBAYYA S.S.A., *Titanium nitride-based CMOS-compatible TE-pass and TM-pass plasmonic polarizers*, IEEE Photonics Technology Letters **28**(3), 2016, pp. 367–370, DOI: 10.1109/LPT.2015.2496380.
[29] HASENICK B., *The increasing importance of extinction ratio in telecommunications*, <https://www.lightwaveonline.com> (October 2005).
[30] KISH P., *The Effect of Network Cabling on Bit Error Rate Performance*, Nordx/CDT White Paper, 2000.
[31] COMSOL Multiphysics, 5.3 a, 2014.
[32] SALZBERG C.D., VILLA J.J., *Infrared refractive indexes of silicon germanium and modified selenium glass*, Journal of the Optical Society of America **47**(3), 1957, pp. 244–246, DOI: 10.1364/JOSA.47.000244.
[33] TAN C.Z., *Determination of refractive index of silica glass for infrared wavelengths by IR spectroscopy*, Journal of Non-Crystalline Solids **223**(1–2), 1998, pp. 158–163, DOI: 10.1016/S0022-3093(97)00438-9.
[34] NAIK G.V., SHALAEV V.M., BOLTASSEVA A., *Alternative plasmonic materials: beyond gold and silver*, Advanced Materials **25**(24), 2013, pp. 3264–3294, DOI: 10.1002/adma.201205076.
[35] CHROSTOWSKI L., HOCHBERG M., *Silicon Photonics Design: From Devices to Systems*, Cambridge University Press, 2015.
[36] LI C., DAI D., *Compact polarization beam splitter for silicon photonic integrated circuits with a 340-nm-thick silicon core layer*, Optics Letters **42**(21), 2017, pp. 4243–4246, DOI: 10.1364/OL.42.004243.
[37] HUANG Y., TU Z., YI X., LI Y., WANG X., *Polarization beam splitter based on cascaded step-size multimode interference coupler*, Optical Engineering **52**(7), 2013, article no. 077103, DOI: 10.1117/1.OE.52.7.077103.

[38] Liu L., Deng Q., Zhou Z., *Manipulation of beat length and wavelength dependence of a polarization beam splitter using a subwavelength grating*, Optics Letters **41**(21), 2016, pp. 5126–5129, DOI: 10.1364/OL.41.005126.
[39] Bai B., Liu L., Chen R., Zhou Z., *Low loss, compact TM-pass polarizer based on hybrid plasmonic grating*, IEEE Photonics Technology Letters **29**(7), 2017, pp. 607–610, DOI: 10.1109/LPT.2017.2663439.
[40] Wu S., Hao J., Zhao Z., Yao X.S., *Low loss and high extinction ratio all-silicon TM-pass polarizer with reflection removal enabled by contra-mode conversion Bragg-gratings*, Optics Express **29**(17), 2021, pp. 27640–27652, DOI: 10.1364/OE.432807.
[41] Saber M.G., Plant D.V., Abadía N., *Broadband all-silicon hybrid plasmonic TM-pass polarizer using bend waveguides*, AIP Advances **11**(4), 2021, article no. 045219, DOI: 10.1063/5.0044490.
[42] Prakash C., Sen M., *Optimization of silicon-photonic crystal (PhC) waveguide for a compact and high extinction ratio TM-pass polarization filter*, Journal of Applied Physics **127**(2), 2020, article no. 023101, DOI: 10.1063/1.5130160.
[43] Hu X., Wang J., *Ultrabroadband compact graphene–silicon TM-pass polarizer*, IEEE Photonics Journal **9**(2), 2017, article no. 7101310, DOI: 10.1109/JPHOT.2017.2672901.
[44] Yuan S., Wang Y., Huang Q., Xia J., Yu J., *Ultracompact TM-pass/TE-reflected integrated polarizer based on a hybrid plasmonic waveguide for silicon photonics*, [In] *11th International Conference on Group IV Photonics* (*GFP*), IEEE, 2014, pp. 183–184, DOI: 10.1109/Group4.2014.6961981.
[45] Zhou W., Tong Y., Sun X., Tsang H.K., *Ultra-broadband hyperuniform disordered silicon photonic polarizers*, IEEE Journal of Selected Topics in Quantum Electronics **26**(2), 2020, article no. 8201109, DOI: 10.1109/JSTQE.2019.2938069.
[46] Xu Z., Lyu T., Sun X., *Interleaved subwavelength gratings strip waveguide based TM pass polarizer on SOI platform*, IEEE Photonics Journal **12**(2), 2020, article no. 4900110, DOI: 10.1109/JPHOT.2020.2968570.
[47] Chen R., Bai B., Zhou Z., *Low-loss hybrid plasmonic TM-pass polarizer using polarization-dependent mode conversion*, Photonics Research **8**(7), 2020, pp. 1197–1202, DOI: 10.1364/PRJ.392654.
[48] Saber M.G., Abadía N., Plant D.V., *CMOS compatible all-silicon TM pass polarizer based on highly doped silicon waveguide*, Optics Express **26**(16), 2018, pp. 20878–20887, DOI: 10.1364/OE.26.020878.
[49] Kim D.W., Lee M.H., Kim Y., Kim K.H., *Ultracompact transverse magnetic mode-pass filter based on one-dimensional photonic crystals with subwavelength structures*, Optics Express **24**(19), 2016, pp. 21560–21565, DOI: 10.1364/OE.24.021560.
[50] Zhang J., Yang J., Liang L., Wu W., *Broadband TM-mode-pass polarizer and polarization beam splitter using asymmetrical directional couplers based on silicon subwavelength grating*, Optics Communications **407**, 2018, pp. 46–50, DOI: 10.1016/j.optcom.2017.08.044.
[51] Abd-Elkader A.E.-S., Hameed M.F.O., Areed N.F.F., Mostafa H.E.-D., Obayya S.S.A., *Ultracompact AZO-based TE-pass and TM-pass hybrid plasmonic polarizers*, Journal of the Optical Society of America B **36**(3), 2019, pp. 652–661, DOI: 10.1364/JOSAB.36.000652.
[52] Dhingra N., Dell'Olio F., *Ultralow loss and high extinction ratio TM-pass polarizer in silicon photonics*, IEEE Photonics Journal **12**(6), 2020, article 6602311, DOI: 10.1109/JPHOT.2020.3032847.
[53] Guan X., Xu P., Shi Y., Dai D., *Ultra-compact broadband TM-pass polarizer using a silicon hybrid plasmonic waveguide grating*, [In] *Asia Communications and Photonics Conference 2013*, OSA Technical Digest (online), Optica Publishing Group, 2013, paper ATh4A.2, DOI: 10.1364/ACPC.2013.ATh4A.2.
[54] Bai B., Yang F., Zhou Z., *Demonstration of an on-chip TE-pass polarizer using a silicon hybrid plasmonic grating*, Photonics Research **7**(3), 2019, pp. 289–293, DOI: 10.1364/PRJ.7.000289.
[55] Selvaraja S.K., Jaenen P., Bogaerts W., Van Thourhout D., Dumon P., Baets R., *Fabrication of photonic wire and crystal circuits in silicon-on-insulator using 193-nm optical lithography*, Journal of Lightwave Technology **27**(18), 2009, pp. 4076–4083, DOI: 10.1109/JLT.2009.2022282.

[56] HEIL S.B.S., LANGEREIS E., ROOZEBOOM F., VAN DE SANDEN M.C.M., KESSELS W.M.M., *Low-temperature deposition of TiN by plasma-assisted atomic layer deposition*, Journal of the Electrochemical Society **153**(11), 2006, G956, DOI: 10.1149/1.2344843.

[57] RITALA M., LESKELÄ M., DEKKER J.P., MUTSAERS C., SOININEN P.J., SKARP J., *Perfectly conformal TiN and Al_2O_3 films deposited by atomic layer deposition*, Chemical Vapor Deposition **5**(1), 1999, pp. 7–9, DOI: 10.1002/(SICI)1521-3862(199901)5:1%3C7::AID-CVDE7%3E3.0.CO;2-J.

[58] SELVARAJA S.K., *Wafer-Scale Fabrication Technology for Silicon Photonic Integrated Circuits*, PhD Thesis, Ghent University, Belgium, 2011.

[59] TANUSHI Y., KITA T., TOYAMA M., SEKI M., KOSHINO K., YOKOYAMA N., OHTSUKA M., SUGIYAMA A., ISHITSUKA E., SANO T., HORIKAWA T., YAMADA H., *Uniform characteristics of Si-wire waveguide devices fabricated on 300 mm SOI wafers by using ArF immersion lithography*, [In] *10th International Conference on Group IV Photonics*, IEEE, 2013, pp. 105–106, DOI: 10.1109/Group4.2013.6644448.

[60] SELVARAJA S.K., BOGAERTS W., DUMON P., VAN THOURHOUT D., BAETS R., *Subnanometer linewidth uniformity in silicon nanophotonic waveguide devices using CMOS fabrication technology*, IEEE Journal of Selected Topics in Quantum Electronics **16**(1), 2010, pp. 316–324, DOI: 10.1109/JSTQE.2009.2026550.

Received December 18, 2021
in revised form April 21, 2022